Available online at www.sciencedirect.com
SCIENCE DIRECT®
International Journal of Heat and Mass Transfer 47 (2004) 1391–1401
International Journal of HEAT and MASS TRANSFER
www.elsevier.com/locate/ijhmt

The impact of compressible liquid droplet on hot rigid surface

Anton V. Chizhov [a,b,*], Kazuyoshi Takayama [a]

[a] Shock Wave Research Center, Institute of Fluid Science, Tohoku University, 1-1-2 Katahira, Aoba-ku, Sendai 980-77B, Japan
[b] Ioffe Physico-Technical Institute of RAS, 26 Politekhnicheskaya str., St.-Petersburg 194021, Russia

Received 16 December 2002; received in revised form 25 April 2003

Abstract

The processes arising when a high-velocity liquid nitrogen drop impacts a hot rigid wall have been studied by means of numerical simulation. An extremely thin near-wall layer of fluid undergoing heating and liquid–vapor phase transition is clearly distinguished in the droplet, the rest of the liquid remaining cold. A model for the layer, based on the reduced compressible Navier–Stokes equations with a two-phase equation of state, has been constructed and adjusted to the known model for the cold liquid part of the drop, based on the barotropic liquid Lagrangian equations with the Tait equation of state. A predictor-corrector finite-difference scheme for the thin layer equations has been devised and coupled with the finite-element method for the barotropic liquid. Drop shapes and flow field distributions in the layer have been obtained for the impacts of nitrogen droplets of different sizes with an initial velocity 186 m/s and different wall temperatures. The influence of the vapor layer on the drop has been analyzed. The heat flux on the wall has been calculated. An analytic formula has been derived for the heat flux, which is in agreement with the calculations for droplets up to 0.1 mm radius.

Keywords: Compressible droplet impact; High-speed impact; Vapor layer; Shock waves; Spray cooling

1. Introduction

While the interaction between liquid sprays and solid objects occurs in a wide variety of industrial and environmental applications, our understanding of the mechanisms involved in the process is far from complete. Of fundamental importance to such processes is the hydrodynamic and thermodynamic behavior of individual droplets, which affect a solid surface. Comprehensive reviews on the impacts of drops on obstacles can be found in [1–4]. However, impacts at the velocities comparable with sound speed are not prevalent.

A high-speed droplet impact on a cold surface was investigated experimentally, analytically and numerically in the works referred to in [3,8]. The present work is aimed at the aspects of an impact on a hot surface. One of the most important parameters of such an impact is the heat transferred through the wall to the fluid. This heat may cause a thermal shock on the hot solid material [6]. Alternatively, this energy can be used to increase the temperature of the liquid and to vaporize liquid from the droplet base. If the heat transfer rate is large enough during the impact, liquid vaporizing from the base of the droplet can form a "cushion" of vapor between the wall and the liquid phase, which may be capable of repelling the droplet from the substrate. If no direct contact between the liquid and the substrate occurs, the impact is said to be a film boiling impact [7]. The film boiling impact has been thoroughly studied in the works [4,5] for the impact velocities up to tens meters per second. An impact at velocity comparable with the sound speed in droplet liquid differs by the influence of liquid compressibility on ongoing processes. At high pressure there is no distinct phase boundary between liquid and vapor. That is why the term film boiling is not applicable in this case. Nevertheless, as before, the main processes occur in a thin near-wall layer.

* Corresponding author. Address: Shock Wave Research Center, Institute of Fluid Science, Tohoku University, 1-1-2 Katahira, Aoba-ku, Sendai 980-77B, Japan.
E-mail address: anton.chizhov@pop.ioffe.rssi.ru (A.V. Chizhov).

0017-9310/$ - see front matter
doi:10.1016/j.ijheatmasstransfer.2003.05.001

Experimental study of processes that occur during high-speed impact is hardly available due to the convexity and non-transparency of small droplets, as well as the great difference of drop and vapor layer scales.

In the study we consider nitrogen drops (at initial temperature $T_0 = 70$ K) impacting a flat rigid wall (heated to temperature, T_{wall}, from the range up to 600 K) at initial velocity $V_0 = 186$ m/s. Drop sizes (radii) lie in the range from 0.001 to 10 mm.

2. Background and formulation of the problem

We now briefly describe the sequence of events during the impact on a cold wall [8]. At the initial stage, the free surface not contacting with the wall is not deformed. The compression region of the drop is bounded by a shock wave adjacent to the contact spot (Fig. 1a). The reason is that the velocity of the contact spot boundary motion along the wall is infinitely large at the hitting instant, and the disturbances propagating from the wall cannot interact with the free surface. The compression of the liquid is maximal at the contact periphery and continues to increase. One could say that in this stage the droplet accumulates the energy for releasing it into a jet. At the critical instant, the shock wave detaches from the contact area and interacts with the free surface, resulting in a rarefaction wave propagating inside the drop. The free surface starts to deform, and a near-wall high-velocity jet occurs (Fig. 1b). The time of jet formation depends mostly on the viscosity of the liquid and less on the surface tension. The jet tip velocity along the wall far exceeds the impact velocity. When the shock wave approaches the top of the drop, the rarefaction wave, which follows the shock wave, causes the formation of a toroidal cavitation area with the cross-section shown in Fig. 1c. At the final stage of interaction, the expansion wave collapses at the symmetry axis, and a vast cavitation area forms (Fig. 1d), with the maximum of rarefaction located near the axis. Then, the drop splashes. Estimations of the spreading time, the jet velocity, the maximum pressure and the force on the wall can be found in [8] for water drops. It was also found that the liquid flow outside the jet is determined by the initial velocity only, because viscous and surface effects depending on drop size are negligible far from the jet. In contrast, they might be crucial for the jet formation instant and the jet tip propagation velocity.

When impacted on a hot wall, the liquid near the contact spot is heated and transforms to vapor (Fig. 2). Due to the short impact time and the comparatively low heat conductivity, the vapor layer thickness is some orders smaller than the drop size. The layer accumulates energy by heating and may be able to push the liquid back. Let us briefly consider the results obtained using a 1D model, published in [11]. As observed, in contrast to 2D (axisymmetric) case, a 1D drop can be repelled from the wall even in a "cold" impact. For the "hot" impact of the 0.02 mm 1D small nitrogen "drop" with $V_0 = 186$ m/s, $T_{wall} = 600$ K, it was obtained that vapor layer expansion increases the amplitude of the shock wave. Hence, the drop moves in the backward direction with a higher velocity than in a "cold" impact. During the initial stage of the impact of a comparatively big 2 mm drop the layer energy is much less than the initial drop

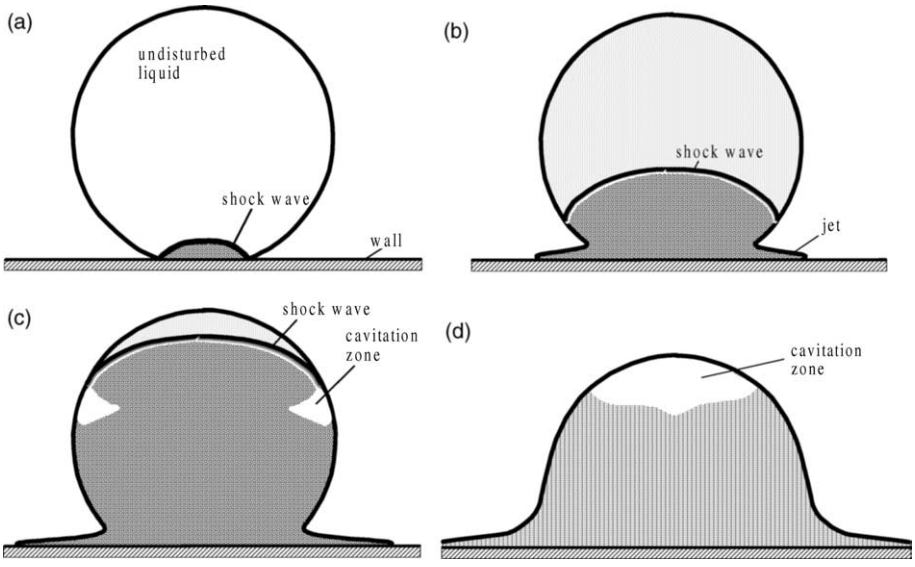

Fig. 1. The sequence of events during the droplet impact on a cold surface.

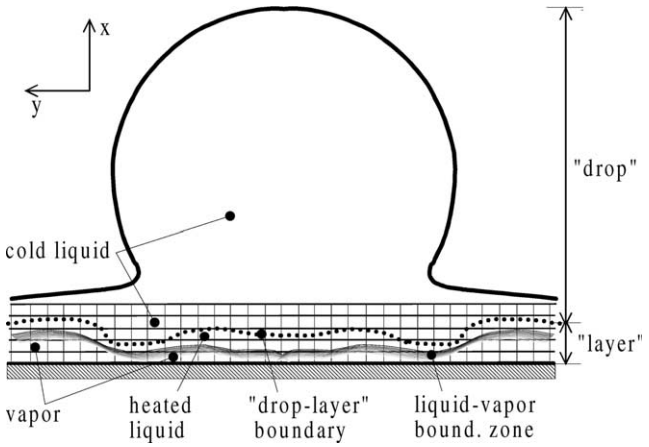

Fig. 2. A schematic of a droplet impact on a hot surface.

kinetic energy. Hence, the layer cannot significantly influence the shock wave. However, the propagation time of the wave is long enough for the layer to accumulate energy. Therefore, when the rarefaction wave comes from the free surface to the wall, the layer produces the second compression wave. As soon as this wave reaches the free surface, it provides acceleration, to a fraction of the liquid near the top of the drop, in the reverse direction, which evokes drop disintegration.

In 2D, most of the shock wave energy transfers to the kinetic energy of the radial jet. Therefore, the shock wave cannot produce bouncing and moreover it cannot significantly slow down the drop during a "cold" impact. We can expect that in a "hot" impact the vapor also lose the energy, moving in the radial direction along with the liquid jet. That is to say, regardless of the jet, "cold" and "hot" impacts are to be similar, if the initial velocity is high. In this work, we are checking this assumption, are investigating the interaction between the drop liquid and the layer, and are calculating the heat transferred from the substrate to the fluid.

3. Mathematical model

The construction of the mathematical model of a high-speed impact on a hot surface started with a 1D model based on the complete Navier–Stokes equations accomplished with the two-phase liquid–gas state equation for nitrogen. This model clarified that the time and spatial scales characterizing the flow near the hot surface differ from the scales for the liquid flow in the rest of the droplet. That is why two different mathematical models have been formulated. The first model for the cold liquid borrows from the work [8] concerning droplet impact on a cold surface, where it was tested and found to be in good agreement with experiments. According to this model, the cold liquid in the drop is considered as a barotropic fluid described by the compressible Navier–Stokes equations written in the Lagrangian 2D cylindrical coordinates and by the Tait equation of state. Here the velocity components, the density, the sound speed and the pressure of the cold liquid are denoted as u^{cold}, v^{cold}, ρ^{cold}, a^{cold} and p^{cold}, respectively.

A different mathematical model has been formulated for the thin near-wall domain below the "drop–layer" boundary, shown in Fig. 2, with the following assumptions:

- the height of the vapor layer is small compared with the radius of the droplet (the layer shown in Fig. 2 is enlarged);
- the height of the layer is a smooth function of the radial coordinate;
- the normal to the wall component of the heated fluid velocity is much lower than the initial impact velocity;
- the temperature on the solid surface is constant;
- no temperature discontinuity exists between the solid surface and the fluid;
- radiation heat transfer is negligible;
- the thermal conductivity of the fluid, k, is constant, corresponding to its value for cold densed medium, where heat conduction is considerable;
- an influence of the surrounding medium flow is negligible (as in [8]).

Using the mentioned assumptions and estimating the order of magnitude for the individual terms of the axial momentum equation, we find that it simplifies to

$$\frac{\partial p}{\partial x} = \frac{4}{3}\frac{\partial}{\partial x}\mu\frac{\partial u}{\partial x}, \tag{1}$$

where the x-axis is the axis of symmetry of the drop (y-axis points along the wall), shown in Fig. 2; p is the

pressure; u is the velocity component in x-direction; μ is the viscosity coefficient. For the bulk of the layer, the viscous term on the right-hand part is very small, which leads to the approximate pressure constancy across the layer.

The radial momentum equation and the continuity equation are considered in their complete form:

$$\frac{\partial \rho v}{\partial t}+\frac{\partial \rho uv}{\partial x}+\frac{\partial \rho v^2}{\partial y}+\frac{\rho v^2}{y}+\frac{\partial p}{\partial y} = \frac{\partial}{\partial x}\mu\frac{\partial u}{\partial y}+\frac{\partial}{\partial x}\mu\frac{\partial v}{\partial x}+\frac{4}{3}\frac{\partial}{\partial y}\mu\frac{\partial v}{\partial y}-\frac{2}{3}\frac{\partial}{\partial y}\mu\frac{\partial u}{\partial x}, \quad (2)$$

$$\frac{\partial \rho}{\partial t}+\frac{\partial \rho u}{\partial x}+\frac{1}{y}\frac{\partial \rho vy}{\partial y}=0, \quad (3)$$

where ρ is the density; v is the velocity component in y-direction.

The equation for conservation of thermal energy, neglecting the viscous dissipation terms, is written as

$$\frac{\partial T}{\partial t}+u\frac{\partial T}{\partial x}+v\frac{\partial T}{\partial y}=\frac{k}{\rho C_p}\left(\frac{\partial^2 T}{\partial x^2}+\frac{1}{y}\frac{\partial}{\partial y}y\frac{\partial T}{\partial y}\right), \quad (4)$$

where T is the temperature; $C_p = C_p(\rho, T)$ is the specific heat at constant pressure.

For the viscosity the Sutherlands law was used, $\mu = bT^{3/2}/(T + 106.667\ \mathrm{K})$, where $b = 1.3998 \times 10^{-6}$ $\mathrm{kg\,m^{-1}\,s^{-1}\,K^{-1/2}}$.

3.1. Equation of state

The equation of state for the liquid-gaseous nitrogen $p = p(\rho, T)$ (Fig. 3) and the dependence $C_p = C_p(\rho, T)$ are taken from [10]. Note that for a high-speed impact the characteristic pressure is much higher than the pressure at the critical point. That is why we do not observe a distinct boundary between the liquid and vapor, but a zone of phase transition, marked as the hatched strip in Fig. 2. Indeed, in the considered case of a high-speed impact the maximum pressure can be estimated approximately as $3\rho_0 a_0 V_0$ [8], where $a_0 = 934$ m/s is the sound speed in the initial state at $T_0 = 70$ K, $\rho_0 = 804$ kg/m^3. For instance, for $V_0 = 100$ m/s the corresponding pressure is about 200 MPa. This maximum pressure, originating during the impact, is much higher than the critical point value $p_c = 3.4$ MPa (Fig. 3). That is why the trajectory of states during the impact cannot enter the metastability region, and we do not observe an abrupt but rather a gradual change of phases. The zone of phase transition inside the layer is shown in Fig. 2 as the hatched line.

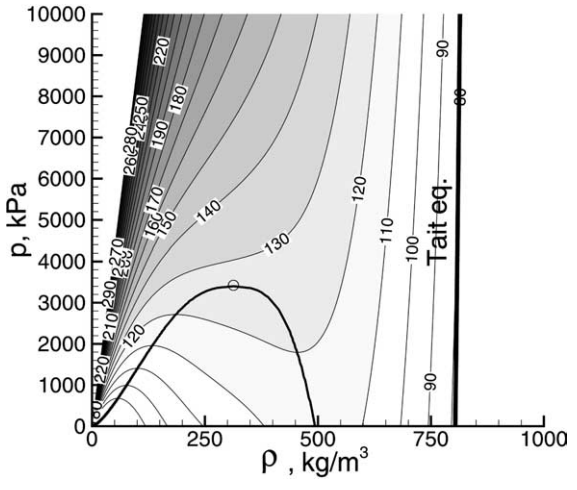

Fig. 3. The state equation for nitrogen is shown as the plot of isolines labeled in Kelvin. Thick lines are the metastability region boundary and Tait equation of state. The small circle marks the critical point.

3.2. Initial and boundary conditions

At the initial moment of an impact the drop is implied to be a liquid ball with the given radius, R_0. The state parameters are the given temperature, T_0, the atmospheric pressure and the corresponding density, ρ_0. The impact velocity is V_0.

No-slip boundary conditions are imposed at the wall, $x = 0$ (Fig. 4); the wall temperature is T_{wall}. The symmetry conditions are set for $y = 0$.

The position of "drop–layer" boundary (Fig. 2), $x = x_l(y)$, is determined by temperature. Namely, it corresponds to the temperature level $T^{\delta}(y) = T^{\mathrm{cold}}(y) + \varepsilon(T_{\mathrm{wall}} - T^{\mathrm{cold}}(y))$, which is close to $T^{\mathrm{cold}}(y)$. Here ε is the small numerical parameter, set to be 0.01; $T^{\mathrm{cold}}(y)$ is the temperature of the cold liquid having undergone the shock wave. On the "drop–layer" boundary, the field disturbances propagating from the cold drop to the layer are described by the cold liquid equations. Hence for $x = x_l(y)$, it is proposed to impose the condition on the Riemann invariant

$$-u + \Pi(p) = -u^{\mathrm{cold}} + \Pi(p^{\mathrm{cold}}), \quad \Pi(p) = \int_0^p \frac{\mathrm{d}p}{\rho a}, \quad (5)$$

where the integral $\Pi(p)$ is calculated at $T = T_0$. The other condition here is $\partial v/\partial x = 0$.

An overlap of the computational domains is implied, the first domain covering the cold liquid, the second one covering the layer. The top boundary of the second domain is "semi-infinite" at $x = x_\infty$, remote from the "drop–layer" boundary, $x = x_l(y)$. Between the "drop–layer" boundary and the top boundary of the "layer domain", the pressure and the velocity are constant across the layer. Hence, the only holding condition for the heat transfer equation necessary is at the top boundary of the "layer domain", which is $\partial T/\partial x = 0$.

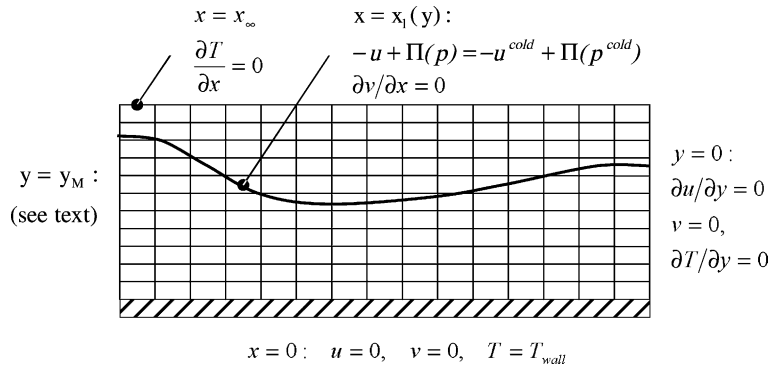

Fig. 4. A schematic of the heated fluid layer computational domain.

The outlet of the layer domain is set at the contact spot contour, $y = y_M$, and then at the tip of the jet. Hard boundary conditions are applied here, if the velocity of the contact spot contour, V_M, is higher than the velocity of the cold liquid along the wall, v^{cold}. The conditions are $\rho = \rho^{\text{cold}}, \quad v = v^{\text{cold}}, \quad u = 0, \quad T(x) = \{T^{\text{cold}}$ if $x > 0$; T^{wall} if $x = 0\}$. When field disturbances reach the outlet boundary, i.e. when $V_M < v^{\text{cold}}$, the conditions are replaced with the soft conditions: $\partial\rho/\partial y = 0$, $\partial u/\partial y = 0$, $\partial v/\partial y = 0$, $\partial T/\partial y = 0$. In the simulations, the negligibly thin edge of the jet was excluded from consideration, the layer domain was shortened.

4. Numerical scheme

To solve the equations for the cold barotropic liquid with a free moving boundary we used the well-proved algorithm [9] based on the Lagrangian description, the finite-element approach combined with a TVD-scheme, the moving unstructured triangular mesh adapting to flow field and the embedded finer adaptive mesh covering the jet origin zone.

To construct a numerical scheme for the hot impact problem (Eqs. (1)–(5)) it is necessary to take into account numerous mathematical properties of the system. Indeed, the main process is the heat transfer across the layer, which is described by the parabolic equation (4) and determines the dominant changes of the medium density. Hence, excluding heat transfer, Eqs. (1)–(3) reveal the properties of the incompressible Navier–Stokes equations, which are of the elliptic and parabolic types. Besides, the condition at the "drop–layer" boundary (5) is governed by the hyperbolic equations for the cold liquid, providing wave-like propagation of field disturbances along the layer. The other computational complexities are caused by the high non-linearity due to the phase transition inside the layer; by the modification of the boundary conditions at the layer onset and by the implicit dependence of pressure and flow fields on the "drop–layer" boundary (5). Fortunately, the simplification made for the normal momentum equation allows outgoing sound speed effects of wave propagation across the layer.

As a result, an implicit finite-difference numerical scheme with a predictor for the heat transfer equation has been proposed. The role of the predictor is to treat the biggest changes of density in the region of phase transition before solving the dynamics equations. That is why on the predictor step Eq. (4) is solved across the layer for the new temperature T^*, and the density ρ^* is predicted, supposing the layer pressure to be equal to the one in the "cold" domain at the "drop–layer" boundary $p^{\text{d}}(y) = p^{\text{cold}}(x_l(y), y)$:

$$\frac{T^*_{i,j} - T^n_{i,j}}{\Delta t} + u^n_{i,j}\left[\frac{\partial T^*}{\partial x}\right]_{i,j} = \frac{k}{\rho^n_{i,j} C^n_{p_{i,j}}}\left[\frac{\partial^2 T^*}{\partial x^2}\right]_{i,j} + \frac{\Delta x}{2}|u^n_{i,j}|\left[\frac{\partial^2 T^*}{\partial x^2}\right]_{i,j},$$

$$\rho^*_{i,j} = \rho(p^{\text{d}}_j, T^*_{i,j}), \quad i = 0, \ldots, N_i, \; j = 0, \ldots, N_j.$$

Here and in the future the superscript n denotes the previous time step; i, j are the node indexes on the rectangular mesh of dimension $N_i \times N_j$. The brackets with subscripts mark the difference derivatives centered at the point corresponding to the subscripts. The term with the mesh cell size Δx as a coefficient is used as an artificial viscosity to construct the upwind approximation of the convection terms. The obtained linear system is solved by the scalar Thomas algorithm. The equation for density may have several solutions; the correct solution is the one closest to $\rho^n_{i,j}$.

Then, by means of linearization and factorization of the left-hand part of the implicit approximation for the complete set of Eqs. (1)–(4) we obtain two block-diagonal linear systems. For that purpose, we consider $(\rho, \rho u, \rho v, T)^{\text{T}}$ as a vector of main variables and factorize the momentum equation (1) as an equation for ρ and the continuity equation (3) for ρu. The values on the new

time step are defined via their increments as $\rho_{i,j}^{n+1} = \rho_{i,j}^{*} + \Delta_{i,j}^{\rho}$, $(\rho u)_{i,j}^{n+1} = (\rho u)_{i,j}^{n} + \Delta_{i,j}^{\rho u}$, $(\rho v)_{i,j}^{n+1} = (\rho v)_{i,j}^{n} + \Delta_{i,j}^{\rho v}$, $T_{i,j}^{n+1} = T_{i,j}^{*} + \Delta_{i,j}^{\mathrm{T}}$. Omitting the index n, for every j, $j = 1, \ldots, N_{j-1}$, we write the linear algebraic system to solve by the block-diagonal Thomas algorithm for the intermediate values ($\widetilde{\Delta}_{i,j}^{\rho}$, $\widetilde{\Delta}_{i,j}^{\rho u}$, $\widetilde{\Delta}_{i,j}^{\rho v}$, $\widetilde{\Delta}_{i,j}^{\mathrm{T}}$):

$$\left[\frac{\partial \widetilde{\Delta}^{p}}{\partial x}\right]_{i+\frac{1}{2},j} - \frac{4}{3}\left[\frac{\partial}{\partial x}\mu\frac{\partial(\widetilde{\Delta}^{\rho u}/\rho)}{\partial x}\right]_{i,j} = -\left[\frac{\partial p}{\partial x}\right]_{i+\frac{1}{2},j} + \frac{4}{3}\left[\frac{\partial}{\partial x}\mu\frac{\partial u}{\partial x}\right]_{i,j},$$

$$\frac{\widetilde{\Delta}_{i,j}^{\rho}}{\Delta t} + \left[\frac{\partial \widetilde{\Delta}^{\rho u}}{\partial x}\right]_{i-\frac{1}{2},j} = -\frac{\rho^{*}-\rho}{\Delta t}\bigg|_{i-\frac{1}{2},j-\frac{1}{2}} - \left[\frac{\partial \rho u}{\partial x}\right]_{i-\frac{1}{2},j} - \frac{1}{y_j}\left[\frac{\partial(\rho v y)}{\partial y}\right]_{i,j} + \frac{\Delta y}{2}|v_{i,j}|\left[\frac{\partial^2 \rho v}{\partial y^2}\right]_{i,j},$$

$$\frac{\widetilde{\Delta}_{i,j}^{\rho v}}{\Delta t} + \left[\frac{\partial(u\widetilde{\Delta}^{\rho v})}{\partial x}\right]_{i,j} - \left[\frac{\partial}{\partial x}\mu\frac{\partial(\widetilde{\Delta}^{\rho v}/\rho)}{\partial x}\right]_{i,j} = -\left[\frac{\partial(\rho v u)}{\partial x}\right]_{i,j} - \frac{1}{y_j}\left[\frac{\partial(y\rho v^2)}{\partial y}\right]_{i,j} + \frac{\Delta y}{2}|v_{i,j}|\left[\frac{\partial^2(\rho v^2)}{\partial y^2}\right]_{i,j} - \left[\frac{\partial p}{\partial y}\right]_{i,j+\frac{1}{2}} + \left[\frac{\partial}{\partial x}\mu\frac{\partial u}{\partial y}\right]_{i,j} + \left[\frac{\partial}{\partial x}\mu\frac{\partial v}{\partial x}\right]_{i,j} + \frac{4}{3}\left[\frac{\partial}{\partial y}\mu\frac{\partial v}{\partial y}\right]_{i,j} - \frac{2}{3}\left[\frac{\partial}{\partial y}\mu\frac{\partial u}{\partial x}\right]_{i,j},$$

$$\frac{\widetilde{\Delta}_{i,j}^{\mathrm{T}}}{\Delta t} + u_{i,j}\left[\frac{\partial \widetilde{\Delta}^{\mathrm{T}}}{\partial x}\right]_{i,j} - \frac{1}{\rho_{i,j}C_{p_{i,j}}}\left[\frac{\partial}{\partial x}k\frac{\partial \widetilde{\Delta}^{\mathrm{T}}}{\partial x}\right]_{i,j} = -u_{i,j}\left[\frac{\partial T}{\partial x}\right]_{i,j} - v_{i,j}\left[\frac{\partial T}{\partial y}\right]_{i,j} + \frac{\Delta y}{2}|v_{i,j}|\left[\frac{\partial^2 T}{\partial y^2}\right]_{i,j} + \frac{k}{\rho_{i,j}C_p i,j}\left(\left[\frac{\partial^2 T}{\partial x^2}\right]_{i,j} + \left[\frac{\partial^2 T}{\partial y^2}\right]_{i,j}\right),$$

where

$$\widetilde{\Delta}^{p} = \frac{\partial p}{\partial \rho}\bigg|_{i,j}^{n}\widetilde{\Delta}^{\rho} + \frac{\partial p}{\partial T}\bigg|_{i,j}^{n}\widetilde{\Delta}^{\mathrm{T}}.$$

Then, for every i, $i = 1, \ldots, N_{i-1}$, the following linear algebraic system is solved

$$\frac{\partial p}{\partial \rho}\bigg|_{i,j}^{n}\Delta^{\rho} + \frac{\partial p}{\partial T}\bigg|_{i,j}^{n}\Delta^{\mathrm{T}} = \Delta\tilde{p},$$

$$\frac{\Delta_{i,j}^{\rho}}{\Delta t} + \frac{\Delta_{i,j}^{\rho u}}{\Delta x} + \frac{1}{y_j}\left[\frac{\partial(y\Delta^{\rho v})}{\partial y}\right]_{i,j} - \frac{\Delta y}{2}|v_{i,j}|\left[\frac{\partial^2 \Delta^{\rho v}}{\partial y^2}\right]_{i,j} = \frac{\widetilde{\Delta}_{i,j}^{\rho}}{\Delta t} + \frac{\Delta_{i-1,j}^{\rho u}}{\Delta x} + \left[\frac{\partial \widetilde{\Delta}^{\rho u}}{\partial x}\right]_{i-\frac{1}{2},j},$$

$$\frac{\Delta_{i,j}^{\rho v}}{\Delta t} + \frac{1}{y_j}\left[\frac{\partial(y\Delta^{\rho v}v)}{\partial y}\right]_{i,j} - \frac{\Delta y}{2}|v_{i,j}|\left[\frac{\partial^2(\Delta^{\rho v}v)}{\partial y^2}\right]_{i,j} = \widetilde{\Delta}_{i,j}^{\rho v},$$

$$\frac{\Delta_{i,j}^{\mathrm{T}}}{\Delta t} + v_{i,j}\left[\frac{\partial \Delta^{\mathrm{T}}}{\partial y}\right]_{i,j} - \frac{k}{\rho_{i,j}C_{p_{i,j}}}\left[\frac{\partial^2 \Delta^{\mathrm{T}}}{\partial y^2}\right]_{i,j} - \frac{\Delta y}{2}|v_{i,j}|\left[\frac{\partial^2 \Delta^{\mathrm{T}}}{\partial y^2}\right]_{i,j} = \widetilde{\Delta}_{i,j}^{\mathrm{T}}.$$

The terms with the coefficient $\Delta y/2|v_{i,j}|$, where Δy is the mesh cell size, are the artificial dissipation terms providing upwind approximation. In the nodes of the "drop–layer" boundary, the linearized boundary condition for the Riemann invariant (5) is calculated within this block-diagonal system, instead of the equation for the momentum component across the layer:

$$\left(\frac{\rho_{i,j}u_{i,j}}{\rho_{i,j}^{*2}} + \frac{a_{i,j}}{\rho_{i,j}^{*}}\right)\Delta_{i,j}^{\rho} - \frac{\Delta_{i,j}^{\rho u}}{\rho_{i,j}^{*}} + \left(\rho_{i,j}^{*}a_{i,j}\left(\frac{\partial p}{\partial T}\right)_{i,j}\right)^{-1}\Delta_{i,j}^{\mathrm{T}} = R_j^{\mathrm{cold}} + \frac{\rho_{i,j}u_{i,j}}{\rho_{i,j}^{*}} + \Pi(p_j^{\mathrm{d}}).$$

The described numerical scheme has been applied after every time step for the "cold" liquid domain. The time step has to satisfy the CFL-condition for the "cold" domain [9].

5. Results

5.1. Numerical parameters and solution convergence

The basic mesh for the simulation was characterized by the least element area set to $10^{-6}R_0^2$ for the finer mesh inserted in the circle near the jet origin and $16\times10^{-6}R_0^2$ for the outer mesh inside the drop. The layer mesh had $\Delta y = 0.005R_0$ and 170 nodes in vertical direction. During simulation, the number of nodes was varying according to the radial layer size, i.e. the radial coordinate of the jet tip. In the vertical direction Δx was increasing according to layer height growth.

The solutions were compared, obtained on three different meshes, which were the basic one and the meshes with characteristic linear sizes 2 and 4 times larger. The solutions are shown in Fig. 5. For the purposes of the present work, the solution on the basic mesh can be accepted as quite accurate. However, for instance, estimations of the jet origination instant and the jet velocity need a sequence of meshes for convergent solution, as used for the cold droplet impact in [8].

5.2. Evolution of drop and layer shapes

For the impact with the parameters $R_0 = 0.01$ mm, $V_0 = 186$ m/s, $T_{\mathrm{wall}} = 600$ K, $T_0 = 80$ K the evolution of the drop shape and the density gradient inside the drop and the layer are illustrated in Fig. 6. The shock wave

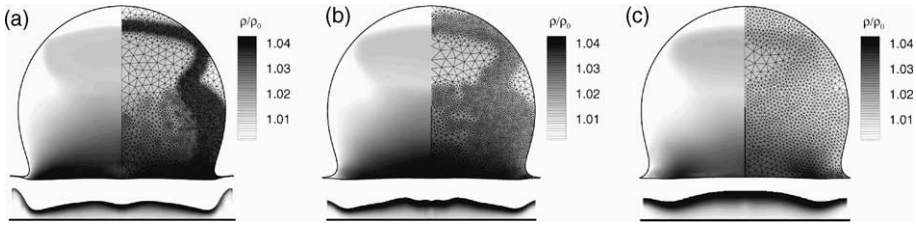

Fig. 5. The solutions obtained on three different meshes are shown at the instant $t = 0.3R_0/V_0$ for the impact with the parameters $R_0 = 0.01$ mm, $V_0 = 186$ m/s, $T_{wall} = 600$ K, $T_0 = 80$ K. The computational domain covering the layer is magnified by a factor of 5. At the observed instant the mesh dimensions were approximately: (a) 200×170, (b) 100×140, (c) 50×80.

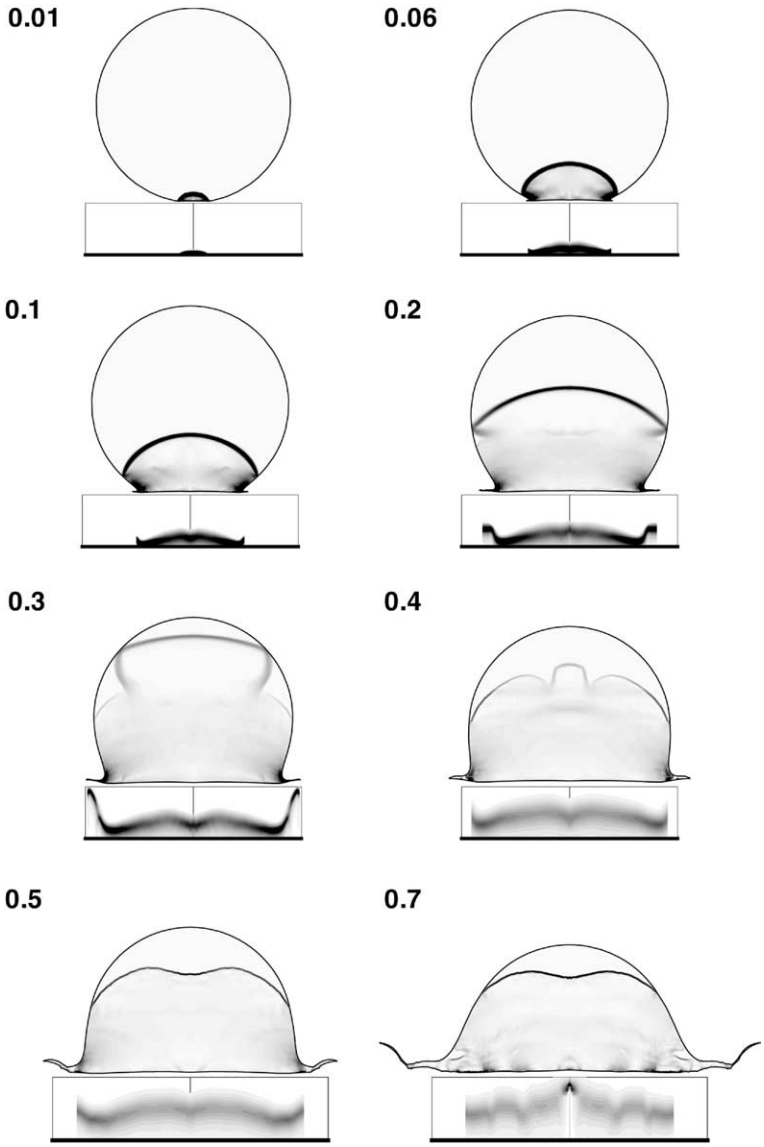

Fig. 6. Impact of the nitrogen drop with $R_0 = 0.01$ mm, $V_0 = 186$ m/s, $T_0 = 80$ K on the hot wall with $T_{wall} = 600$ K. The field of density gradient is shown at $t = 0.01$, 0.06, 0.1, 0.2, 0.3, 0.4, 0.5, 0.7 R_0/V_0.

moves towards the apex (at $t = 0.01$, 0.06, 0.1, 0.2, 0.3 R_0/V_0), interacts with the free surface and evokes the rarefaction wave spreading towards the wall ($t = 0.4$, 0.5, 0.7 R_0/V_0). Meanwhile, the layer height increases slowly until the origination of the jet (at $t = 0.06R_0/V_0$), and then it starts to grow quickly under the jet, due to pressure reduction there. The phase transition zone corresponds to the dark zone of steep density gradient in Fig. 6, and is just below the layer boundary. The vapor is much more rarefied under the jet (e.g. see Fig. 6, $t = 0.2R_0/V_0$), causing lower temperature gradient (see Fig. 7). Hence, the heat flux from the wall under the jet is negligible in the total transferred heat.

Concerning the influence of the layer on the droplet, we see that the expansion of the heated vapor increases the pressure in the cold liquid and shifts the drop a little away from the wall. More evident is the influence of the layer on the jet because of its lower inertia (see Fig. 6 for $t = 0.5$ and 0.7 R_0/V_0).

5.3. Impacts of droplets of different sizes

As mentioned above, the influence of the vapor on the drop depends on the ratio of energies of the drop and the vapor. In turn, the energies depend on the drop radius. Let us compare the density distribution at one instant $t = 0.3R_0/V_0$ for the drops of different sizes: $R_0 = 1$, 0.01 mm and 1 μm (Fig. 7). Fig. 7 shows that for 1 μm drop the layer thickness reaches $0.08R_0$, whereas for 1 mm drop it is less than $0.02R_0$, thus the ratio of the layer thickness to the drop radius is relatively thicker for the case of smaller drop. What is the reason? Small radius provides proportionally small heating time. The layer thickness is changing approximately as a square root of the heating time or as a square root of the radius. That is why the ratio of the layer thickness to the drop radius decreases with the radius as $\sim 1/\sqrt{R_0}$. Of course, the absolute value of the layer itself is thicker for bigger drops.

The smaller the drop, the greater the ratio of the accumulated thermal energy to the kinetic energy of the drop. In spite of the fact, even in the small drops, the layer cannot significantly force the shock wave, propagating in liquid (see Fig. 7 for 1 μm drop), because most of the potential energy transfers to the kinetic energy of the radial jet.

For rather big drops, the characteristic time of layer growth is much less than the time of wave propagation. In the solutions at obtained later times, the layer grows slowly, and the process evolves with the complicated shape of the layer boundary (see Fig. 6 for $t = 0.7R_0/V_0$, Fig. 7 for $R_0 = 1$ mm). The flow might become unstable. The authors suppose that the instability can be explained by composing the equation for the vorticity $\xi = \partial v/\partial x - \partial u/\partial y$. After estimating and extracting the main terms, the equation takes form

$$\frac{\partial \xi}{\partial t} = \frac{1}{\rho^2}\frac{\partial p}{\partial y}\frac{\partial \rho}{\partial x}.$$

Hence, having the steep density gradient $\partial\rho/\partial x$ in the phase transition zone, the pressure inhomogeneity along the layer (characterized by the derivative $\partial p/\partial y$) may lead to origination of vortexes in the flow field

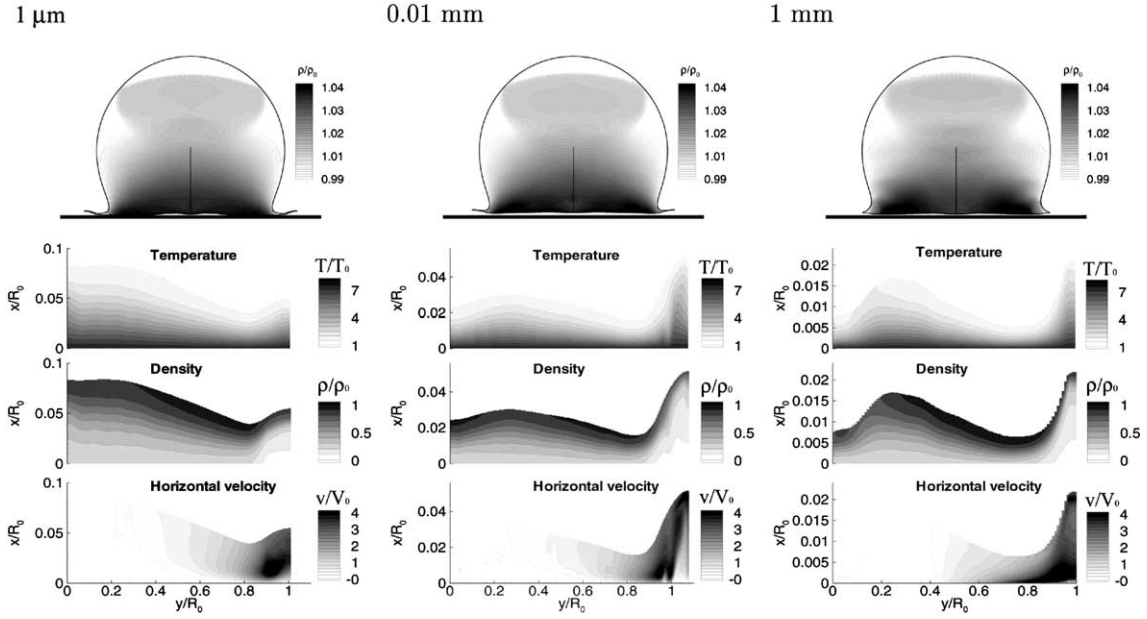

Fig. 7. The distribution of density inside the drop; of temperature, density and horizontal velocity inside the right half of heated fluid layer for drops of different sizes ($R_0 = 0.001$, 0.01, 1 mm) at $t = 0.3R_0/V_0$ ($V_0 = 186$ m/s, $T_{wall} = 600$ K).

($\partial\xi/\partial t \neq 0$). Such instability cannot be treated properly in the simulations.

5.4. Impacts on walls at different temperatures

The impact on the wall with $T_{\text{wall}} = 600$ K (Fig. 7, middle) is accompanied by the phase transition from liquid to vapor along the whole length of the layer of the heated liquid. As mentioned before, such phase transition occurs above the critical point, and no distinct boundary exists between the liquid and the vapor. In the case of lower temperature, $T_{\text{wall}} = 140$ K, a distinct phase boundary is seen in Fig. 8 as the density gradient under the origin of the jet, separating the liquid under the bulk of drop and the vapor on periphery. The phase transition does not occur under the bulk of the drop because of high pressure. It takes place under the jet only, where the pressure is much lower. Naturally, the layer is thinner in the case of lower wall temperature, the influence of the layer on the jet is less noticeable.

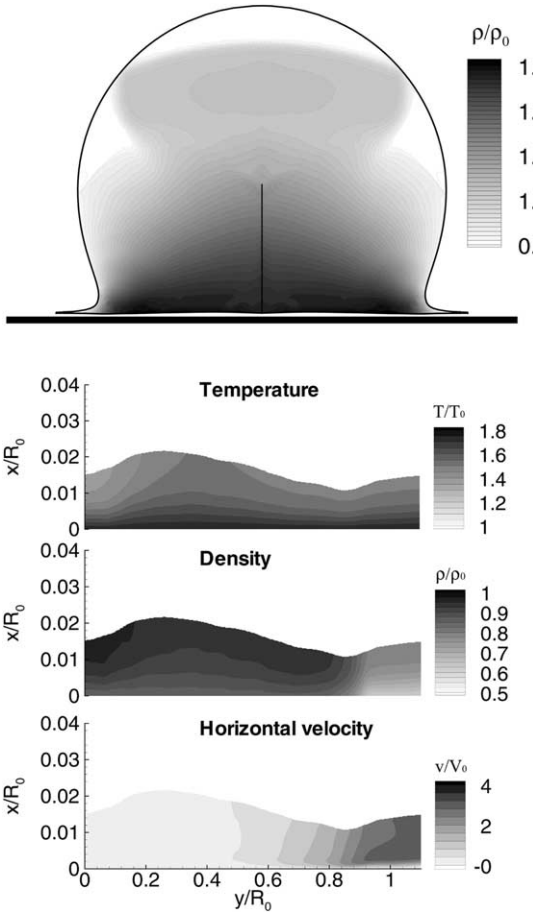

Fig. 8. The impact of $R_0 = 0.01$ mm drop on the wall with $T_{\text{wall}} = 140$ K at $V_0 = 186$ m/s. Density field inside the drop (top) and the temperature, density and horizontal velocity distributions inside the right half of layer (bottom) at $t = 0.3R_0/V_0$ are shown. Compare with the middle figure of Fig. 7.

5.5. Estimations of heat flux through the wall

For the technologies of surface cooling and film growing by means of droplet impact, the important parameter is the heat flux through the wall [7]. In simulations, we can calculate the temperature history for given parameters of impact. For limited parameter ranges an analytic formula can be derived as well. For this purpose, according to numerical results, we suppose that the specific heat flux is substantial on the contact area limited by the jet origin zone. It appears so, because the pressure and the vapor density under the jet are low, which results in low heat conductivity and low temperature gradient. In contrast, under the bulk of drop we can neglect convection of the vapor near the wall. Then, we suppose that the heat transfer is described by the one-dimensional heat transfer equation.

Further analysis is based on the above assumptions. As assumed, the efficient contact area is limited by the jet origin zone, which is approximately equal to the cross-section of the imaginary spherical drop by the plane surface. Considered from this geometrical point of view, the radius of the spot scaled to the drop radius, $\tilde{y}_M$, is a function of the non-dimensional time, $\tilde{t} = tV_0/R_0$, i.e. $\tilde{y}_M = \sqrt{R_0^2 - (R_0 - V_0 t)^2}/R_0 = \sqrt{2\tilde{t} - \tilde{t}^2}$. That is why, to calculate the total heat transferred through the wall $Q(\tilde{t})$ we integrate the specific heat flux $q = -k\partial T/\partial x$ over the contact spot and time:

$$Q(\tilde{t}) = -2\pi R_0^2 \int_0^{\tilde{t}} \int_0^{\tilde{y}_M(\tilde{t})} k \left.\frac{\partial T}{\partial x}\right|_{x=0} \tilde{y}\,\mathrm{d}\tilde{y}\,\mathrm{d}\tilde{t}. \tag{6}$$

The temperature as a solution of the 1D heat transfer equation is given in [12] as $T = T_0 + (T_{\text{wall}} - T_0)(1 - \operatorname{erf}(x/2\sqrt{at}))$, where the thermal diffusivity, $a = k/(\rho_0 C_p)$, is supposed to be constant. The corresponding temperature gradient at the wall is as follows:

$$\left.\frac{\partial T}{\partial x}\right|_{x=0} = -\frac{T_{\text{wall}} - T_0}{\sqrt{\pi a t}} = -(T_{\text{wall}} - T_0)\sqrt{\frac{V_0}{\pi a R_0 \tilde{t}}}.$$

Thus, we obtain

$$\frac{Q(\tilde{t})}{E_0^k} = \frac{3}{2}(T_{\text{wall}} - T_0)\sqrt{\frac{\pi k C_p}{\rho_0 V_0^5 R_0}} f(\tilde{t}),$$

where

$$f(\tilde{t}) = \int_0^{\tilde{t}} \int_0^{\sqrt{2t' - t'^2}} \tilde{y}/\sqrt{t' - 1 + \sqrt{1 - \tilde{y}^2}}\,\mathrm{d}\tilde{y}\,\mathrm{d}t'. \tag{7}$$

Here the initial kinetic energy, $E_0^k = 2/3\pi\rho_0 V_0^2 R_0^3$ is used as a scale.

The evolution of the non-dimensional heat $f(\tilde{t})$ denoted as Q/Q_0 is shown in Fig. 9A, where $Q_0 = 2(T_{\text{wall}} - T_0)\sqrt{\pi R_0^5 k \rho_0 C_p / V_0}$. Comparison of the heat calculated by Eq. (7) with the one obtained by 2D simulations shows a good agreement for the impacts of droplets smaller than 0.1 mm (Fig. 9B). The agreement depends on the droplet size but not on the wall temperature. Apparently, the disagreement for the rather big drops can be explained by the contribution of convection in the heat transfer. Really, during the initial stage of the layer growth, the rate of layer enlargement is close to the sound speed; hence, acceleration of the cold liquid by the vapor is hardly possible. In contrast, in later stages of the big drop impact, liquid near the wall accelerates and expands. It results in a decrease of the heat flux.

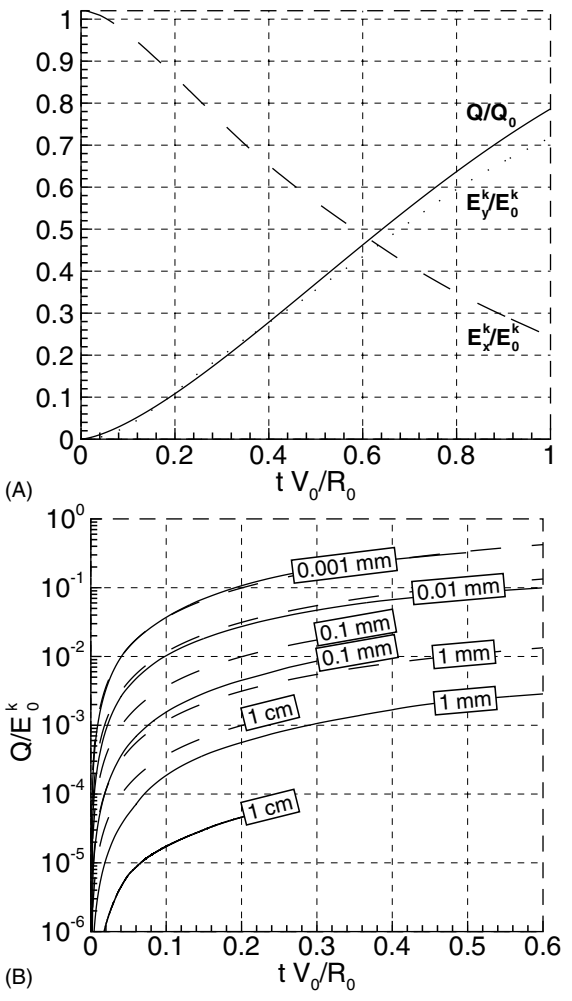

Fig. 9. (A) Evolution of the relative heat transferred through the wall, Q/Q_0, the kinetic energy E_x^k/E_0^k in axial direction and the kinetic energy in radial direction E_y^k/E_0^k. (B) Comparison of the estimations of the heat through the wall, Q/E_0^k, made by Eq. (7) (dashed lines) with Q/E_0^k obtained by 2D simulations (solid lines) for the four impacts of 1 μm, 0.01, 0.1, 1 mm and 1 cm radius droplets with the parameters $V_0 = 186$ m/s, $T_{\text{wall}} = 600$ K.

Fig. 9A shows the decreasing kinetic energy in axial direction and the corresponding increasing kinetic energy in radial direction, which means transformation of the flow towards the wall to the jet motion. Both energies are under weak influence of the heat transfer parameters. The role of the heat transfer can be characterized by the ratio of the decrease rate of the total kinetic energy towards the wall $\dot{E}_x^k$ to the total heat flux from the wall $\dot{Q}$. For instance, for small drop of 0.01 mm radius $\dot{E}_x^k/\dot{Q} = 6$, whereas for 1 mm drop it rises up to 250.

The main conclusion that follows from Eq. (7) is that the heat transfer through the wall for droplets of about 1 mm radius and less depends on the droplet size as $R_0^{5/2}$ and on the velocity as $V_0^{-1/2}$. That is why, the formula (7) allows generalizing the results of simulations for arbitrary but limited parameters of the impacts. In addition, this formula helped to recognize the contribution of convection in the heat transfer. Besides, the agreement of the analytical and numerical models partly justifies adequacy of the mathematical model of the layer.

5.6. Force acting on the wall

The important parameter for the estimation of erosion of solid surfaces is the force of fluid influence on wall. In contrast to the heat flux, the force is substantial on the periphery of the contact spot, i.e. under the jet. In calculations for the impact of $R_0 = 0.01$ mm drop with $V_0 = 186$ m/s on the hot surface with $T_{\text{wall}} = 600$ K, the maximum force integrated over a contact spot was 2 times greater than that in the case of cold impact. The difference increased with radius and wall temperature.

6. Conclusion

The present work studied the main physical effects taking place during the impact of the liquid drop on the heated solid surface. The proposed mathematical model and the numerical scheme for the thin heated fluid layer allowed us to obtain and analyze the detailed flow fields at the initial stages of the impact.

The results obtained showed that during the impact of nitrogen droplets larger than 0.01 mm radius with the velocity of the order of 100 m/s no bouncing occurs, but the almost inertialess tip of the jet can be pushed off the surface by the vapor layer. The reason found is the dominant transformation of the initial kinetic energy and the energy of the heated vapor into the radial jet motion. That is why the processes in the main part of the drop are similar to those during the impact on the cold surface, but near the wall the supersonic jet of vapor appears, and influences the liquid jet.

The heat flux cooling the wall has been calculated. For estimation of the heat flux for small droplets, an analytical formula has been derived. The analytical formula has been justified through numerical simulation.

Taking into account the difficulties of experimental study due to very small scales (e.g. of the order of 10^{-5} m and 10^{-7} s for 1 mm drop) we conclude that the present model is a useful instrument to study high-speed impacts of droplets on either cold or hot surface.

Acknowledgements

This study has been supported by the Japan Society for the Promotion of Sciences. The first author thanks Dr. A. Orlova-Kukushkina and Mr. A. Budovskiy for insightful comments on the manuscript.

References

[1] C. Preece, Erosion, Academic Press, New York, 1979, pp. 1–450.
[2] M. Rein, Phenomena of liquid drop impact on solid and liquid surfaces, Fluid Dyn. Res. 12 (1993) 61–93.
[3] M. Lesser, J. Field, The impact of compressible liquids, Annu. Rev. Fluid Mech. 15 (1983) 97–122.
[4] D.J.E. Harvie, D.F. Fletcher, A hydrodynamic simulation of droplet impacts on hot surfaces. Part I: Theoretical model, Int. J. Heat Mass Transfer 44 (2001) 2633–2642.
[5] D.J.E. Harvie, D.F. Fletcher, A hydrodynamic simulation of droplet impacts on hot surfaces. Part II: Validation and applications, Int. J. Heat Mass Transfer 44 (2001) 2643–2659.
[6] A.A. Deom, A. Luc, S. Amara, D.L. Balageas, Towards more realistic erosion simulation tests for high velocity EM and IR windows, Wear 233 (1999) 13–24.
[7] J.D. Bernardin, C.J. Stebbins, I. Mudawar, Mapping of impact and heat transfer regimes of water drops impinging on a polished surface, Int. J. Heat Mass Transfer 40 (2) (1997) 247–267.
[8] A.V. Chizhov, A.A. Schmidt, Impact of a high-velocity drop on an obstacle, Tech. Phys. 45 (12) (2000) 1529–1537.
[9] Yu.P. Golovachev, E.A. Notkina, A.V. Chizhov, A.A. Schmidt, Simulation of free-surface flows involving shock waves, Comput. Math. Math. Phys. 41 (1) (2001) 151–162.
[10] S. Angus, K.M. de Reuck, B. Armstrong (Eds.), Nitrogen. IUPAC Chemical Data Series; No. 20, International Thermodynamic Tables of the Fluid State, 6, Pergamon Press, Oxford, New York, 1979, pp. 3–244.
[11] A.V. Chizhov, K. Takayama, Simulation of impact and bouncing of nitrogen drop out of heated wall, in: Proceedings of the First International Symposium on Advanced Fluid Information, Sendai, 2001, pp. 563–566.
[12] D.A. Anderson, J.C. Tannehill, R.H. Pletcher, Computational Fluid Mechanics and Heat Transfer, Hemisphere, New York, 1984, pp. 27–28.